

# Volumetric scanning of cells

## Contents

<b>1</b>	<b>Near-field confocal optical spectroscopy (NCOS)</b>	<b>1</b>
<b>2</b>	<b>Optical coherence tomography (OCT)</b>	<b>2</b>
<b>3</b>	<b>Magnetic induction tomography (MIT)</b>	<b>4</b>
<b>4</b>	<b>Nuclear magnetic resonance (NMR) and optical NMR</b>	<b>5</b>
<b>5</b>	<b>Nanofocus computed tomography (nanoCT)</b>	<b>6</b>
<b>6</b>	<b>Conclusions</b>	<b>7</b>

---

## 1 Near-field confocal optical spectroscopy (NCOS)

Due to the wave nature of light, the diffraction limit constrains the spatial resolution of traditional optical microscopy. The point spread function (PSF), the image of a point source, is about 250 nm along transverse directions and about 500 nm along the axial direction [1]. For example, hundreds of proteins, but only a few diffraction limited spots, may fit side by side within a typical 1 micrometer *Escherichia coli* bacterium.

Diverse optical imaging techniques now resolve features below the diffraction limit. Strategies include

- Optical fibers, to limit excitation to volumes smaller than the diffraction limit
- Patterned excitation and nonlinear fluorophore response, to decrease effective PSF
- Sub-pixel localization of fluorophores that switch between dark and light states

Both technological innovation and statistics have made it possible to image structures smaller than the wavelength of light. In near-field confocal optical microscopy (NCOS), an optical fiber is heated and pulled to a minute taper, then aluminum is evaporated onto the sides of the fiber to prevent leakage of the light. A feedback mechanism prevents the delicate tip from crashing into the sample, and then the tip is rastered across the sample to build up an image. This can prove difficult for biological samples because they are often wet and uneven; nevertheless, progress has been made to image neurons, muscle cells, and other biological samples [2, 3].

Diverse super-resolution optical microscopy techniques take advantage of photo-switchable fluorophores and stochastic, rather than rastered, reconstruction of whole images. In this case, if  $\Delta$  represents the uncertainty in the position of a fluorophore after a single measurement, then multiple samplings of the position of the fluorophore can give a localization that decreases with the square root of the number of samples as  $\Delta/\sqrt{N}$ . Adjacent fluorophores must be sampled within the Nyquist resolution  $\Delta_{\text{Nyquist}} = 2/N^{1/D}$  (where  $D$  is the dimensionality of the structure to be imaged) [1], but not excited simultaneously. For example, in stochastic optical reconstruction microscopy (STORM), photo-switchable cyanine dyes are activated and deactivated, to achieve resolutions on the order of 20 nm. [1]

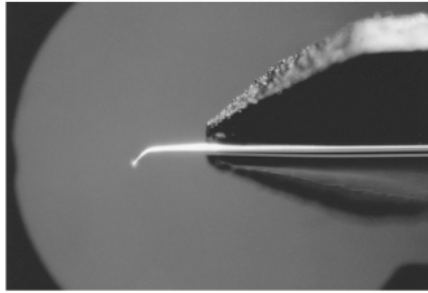


**FIGURE 1**

Tip mount together with a coated, tapered, cantilevered near-field optical fibre element through which an argon ion laser at 488 nm is being transmitted with its polarization preserved. As the light goes through an orifice that is much smaller than the wavelength of the light, there are large losses of intensity, but, nevertheless, as much as 100 nW of intensity from a 100 nm orifice is obtainable when the input intensity is approximately 1 mW. In terms of the mechanical properties of these tips, it has been shown that these tips are at least three orders of magnitude more sensitive to dynamic motions of proteins than silicon cantilevers (see Refs 24 and 25). This dynamic sensitivity extends to the microsecond region, whereas standard AFM silicon cantilevers have monitored only millisecond motions. (Photograph courtesy of Nanonics Ltd.)

Figure 1: An example of a tapered optical fiber used for near-field confocal optical microscopy (NCOS).

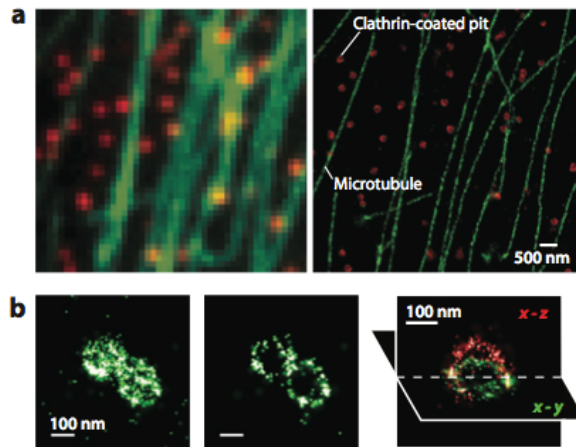


Figure 2: Stochastic optical reconstruction microscopy (STORM) of (a) microtubules and (b) membrane extrusions coated with clathrin.

## 2 Optical coherence tomography (OCT)

Optical coherence tomography (OCT) is an imaging technique that has seen increasing use for biomedical applications especially over the last decade. Given its high sensitivity and low invasiveness, OCT is used to image the eyes of patients with glaucoma, diabetic retinopathy, macular degeneration, macular holes, etc. [4], and the veins of patients with vascular disease.

Optical coherence tomography is analogous to ultrasound imaging, except in this case, light instead of sound is used as the medium that enters the body and backscatters off of structures. The system

measures the time required for light to scatter from structures in the body and return to the detector. To measure distances/elapsed time with high precision, OCT relies on interferometry to measure the time it takes for light to backscatter from tissue microstructures. Detection and demodulation of the interference signal gives the echo delay of the backscattered light from cells.

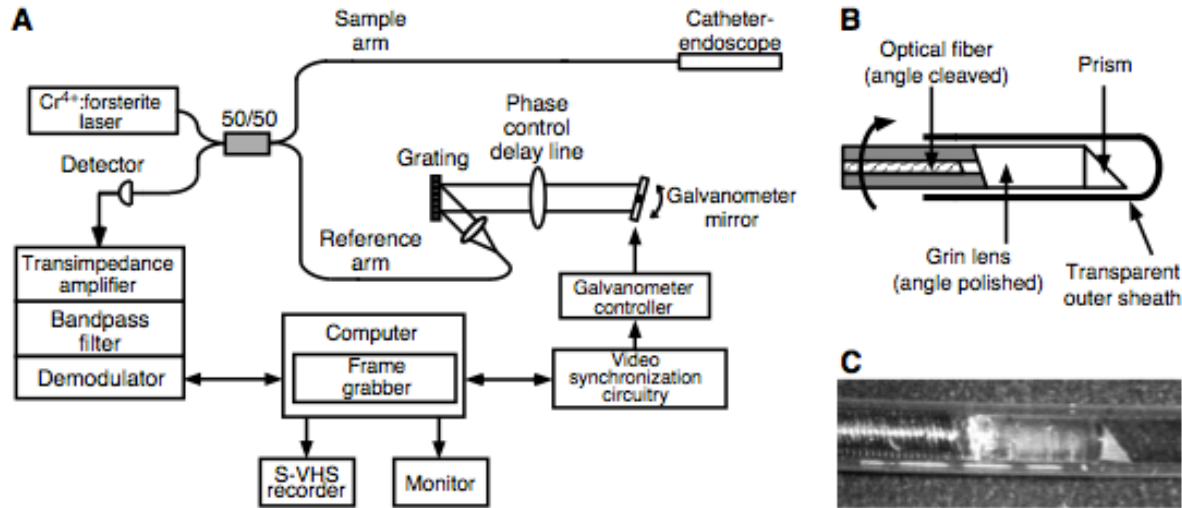


**Fig. 1. (A)** Schematic of the high-speed endoscopic OCT system. **(B)** Schematic of the distal optics of the second-generation OCT catheter-endoscope. The angle cleaving the optical fiber and the angle polishing the GRIN lens minimized internal reflections. **(C)** Photograph of the OCT catheter-endoscope distal optics.

Figure 3: The setup of an optical coherence tomography system. OCT is a Michaelson interferometer, with one arm that projects light into the body, and the other arm on a sensitive delay stage, in order to dynamically tune the path length to measure interference effects. Image taken from [5].

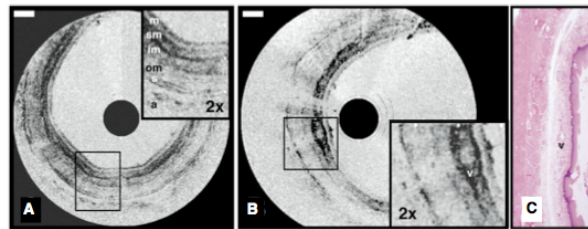


**Fig. 2.** OCT imaging of the rabbit esophagus in vivo (22). **(A)** This image allows visualization of the esophageal layers of the rabbit including the mucosa (m), the submucosa (sm), the inner muscular layer (im), the outer muscular layer (om), the serosa (s), and the adipose and vascular supportive tissues (a). **(B)** A blood vessel (v) is apparent within the submucosa of the esophagus. **(C)** Corresponding histology for (B) (H&E stain). Bars, 500  $\mu$ m.

Figure 4: Image of an *in vivo* rabbit esophagus, taken from [5].

The spatial resolution of OCT depends on the coherence length of the light and thus on the spectral bandwidth of the light source as  $l_c = c/\Delta\nu$ , where  $l_c$  is the coherence length,  $c$  is the speed of light, and  $\Delta\nu$  is some measure of the width of the light spectrum in frequency space. Lower coherence light and larger bandwidths increase the spatial resolution of the features detected by interferometry. For example, using a Kerr-lens mode-locked Ti:sapphire laser, high resolution OCT has achieved  $\approx 2 \mu$ m spatial resolution along the axial direction using a broad spectrum source of 370 nm in bandwidth. [6]

Therefore, some advances in optical coherence tomography have been facilitated by rapid progress in solid state laser technologies over the last couple of decades.

As with the other modalities, a number of modifications and variations of optical coherence tomography exist [6, 7]. These include frequency shifting/signal encoding and autocorrelation, which relies on beat frequencies of added waves with close frequencies and gives a factor of  $\sim 7$  improvement in the axial resolution [7]; both time and Fourier domain OCT, in which the inverse Fourier transform of the backscattered light reveals information along the axial direction [6].

### 3 Magnetic induction tomography (MIT)

Like optical coherence tomography, magnetic induction tomography (MIT) offers a means of non-invasively imaging a sample. Though MIT was developed for industrial applications, some are currently transitioning the technology to biomedical applications. [8] As shown in Fig. 10, a number of the tissues in the body have some conductivity or permittivity due to the dissolved salts and other properties of the tissues.

In magnetic induction tomography, a system of transceivers (coils) inject current into the sample and then detect perturbations in the signal due to the presence of the material. There are a number of techniques related to MIT, likewise based on the premise of injecting currents or applying voltage from an array of transmitters, and then measuring the response currents or voltages after they interact with the sample, such as electromagnetic tomography (EMT).

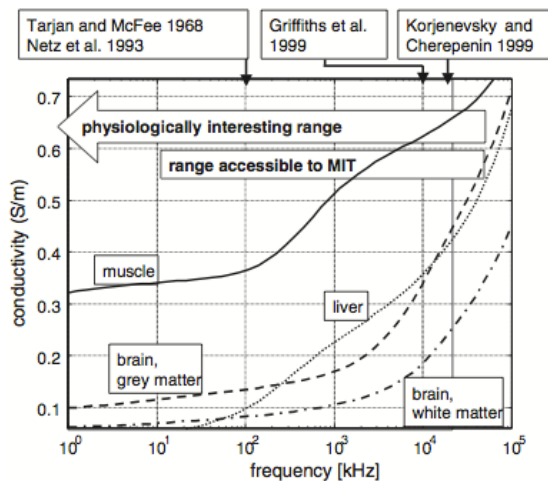


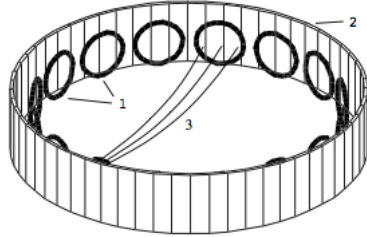
Figure 1. Conductivity spectra of some selected tissues (data taken from Gabriel *et al* 1996).

Figure 5: AC conductivity of various tissues possible to image with MIT, from [8].

MIT requires solution of an inverse problem: given the currents or fields at sampled points on the surface of a volume, what can we infer about the distributions within the volume? Current research challenges include dealing with anisotropies of the body. [9] Many have studied the theoretical signal to noise limits, given a small number of transceivers. [10]

The resolution only about one divided by the square root of the number of transceivers, then further degraded by noise. The spatial resolution depends on the number of independent pairs of transmitters and receivers: if the number of transceivers is  $N$ , then the system can make  $N(N - 1)/2$  measurements. We can calculate the spatial resolution as the diameter of the array of transceivers  $d$  divided by the square root of the number of independent measurements, so  $\lambda = d/(\sqrt{N(N - 1)/2})$ . [8] Image quality

is also limited by the total amount of current injected, the amplitude times the duration of current injection. Especially for live studies, this has an upper bound. For human studies, could inject as much as 10 mA with carbon-hydrogel electrodes with large surface area.[9]



**Figure 1.** Configuration of measuring system for magnetic induction tomography: 1—coils (inductors and detectors), 2—electromagnetic screen, 3—example of unperturbed magnetic induction lines connecting inductor and detector, which are used for backprojection during reconstruction.

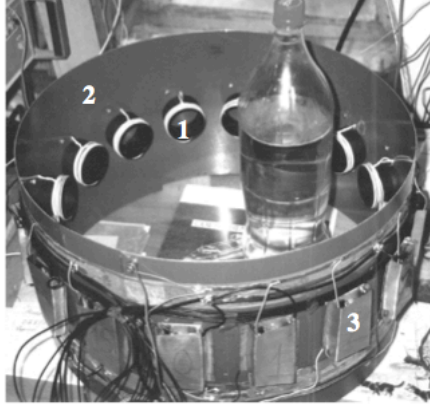


**Figure 2.** External appearance of the measuring system: 1—inductor and detector coils, 2—electromagnetic screen, 3—transmitting and receiving modules. One of the test objects is shown inside the system.

Figure 6: From [11]. An experimental realization of magnetic induction tomography. Korjnevsky et al. imaged a 10 cm wide cylinder filled with saline solution using an array of 16 coils arranged in a circle. They achieved spatial resolution of the sample on the order of  $\sim$ cm.

## 4 Nuclear magnetic resonance (NMR) and optical NMR

The nuclei of the atoms that compose the cell have angular momentum. Since protons are charged, nuclei have an associated magnetic moment  $\vec{\mu}$ . In a static external magnetic field  $\vec{B}$ , magnetic moments have an energy  $\mathcal{H}_Z$  related to their orientation and proportional to the field strength

$$\mathcal{H}_Z = -\vec{\mu} \cdot \vec{B}.$$

Moments that point opposite the field have higher energy than those that point with the field.

Each subvolume of the cell contains many magnetic moments. In an external magnetic field, their energies add together, so that

$$\mathcal{H}_Z = -\sum_i \vec{\mu}_i \cdot \vec{B} = -\vec{M} \cdot \vec{B},$$

where the net magnetization  $\vec{M}$  represents the sum of the magnetic moments within the subvolume. In nuclear magnetic resonance, this Zeeman splitting is used to detect the locations and relative distances/orientations of spins in the solid to be imaged. Thus, NMR can reveal not only structural information but also chemical information, given sufficiently high number of spins. Compared to other detection methods (such as fluorescence), traditional NMR is not as sensitive. [12], due to the thermally distributed low fraction of excited spins at room temperature amidst the static background field.

There are a number of ways to boost the signal to noise and hence the sensitivity of NMR. These include optical pumping, which can transfer angular momenta from photons to nuclei to achieve high polarizations, over 70%! [12]

Recently, several groups have made progress using a nitrogen-vacancy center in a diamond lattice as a small detector of the local spin. [13, 14, 15] Both Staudacher et al. and Mamin et al. use the interesting optical properties of the spin center to read out its spin. Depending on the spin state of the NV center, a microwave can cause a transition to the ground state in which the center is optically active. [15] Unlike the relatively lower signal-to-noise ratios of the thermally polarized spins in traditional NMR, in this case, due to the small detection volume of the spins, finite size or statistical fluctuations in the polarization of the media around the NV center are detectable: for example, if there are on the order of  $N = 10^4$  spins in the vicinity of the NV center, then the typical standard deviation of the spin in the vicinity of the center is  $\sqrt{N} = 100$ , so the population is statistically polarized in some direction; this random transverse polarization rotates with the Larmor frequency under the applied static magnetic field. [15]

Both of these techniques employ some kind of spin echo technique to prevent decoherence of the spins over the time scale of interest. This is a great animation that gives some intuition how RF pulses that modify the state of the spins cause the spins to diverge and then to come back together ([http://en.wikipedia.org/wiki/File:HahnEcho\\_GWM.gif](http://en.wikipedia.org/wiki/File:HahnEcho_GWM.gif)). The point is that different spins precess at different rates due to inhomogeneous effects, and the  $180^\circ$  pulse causes the spins to come back together.

## 5 Nanofocus computed tomography (nanoCT)

The research frontiers of nano focus computed tomography involve synchrotron beam lines and fabrication of higher resolution Fresnel lenses. As discussed, glass lenses can be abstracted to surfaces that cause the wave to constructively interfere in some regions and destructively interfere in other regions. In this case, at the tradeoff of lost power, the lens is able to focus waves (such as X rays) that traditional lenses are not able to perturb.

Fresnel zone plates shifts the problem of spatial resolution onto a fabrication problem: how closely spaced together can we fabricate sufficiently thick features? Fresnel plates often are arranged as concentric rings with decreasing width and increasing radius. The width of innermost feature sets the resolution. [16] In this study, the authors deposited gold on silicon nitride membrane and formed innermost features on the order of 30 nm to meet the Rayleigh resolution of  $38.5 \pm 1.2$  nm. Note that X rays are diffraction limited as well, but since the wavelength of X rays is much smaller than that of visible light (about  $10^4$  smaller), the diffraction limited spot is smaller than that from NCOS.

In addition to Fresnel lens fabrication, others are investigating new X rays sources for imaging, effectively bringing the synchrotron into the lab [18].

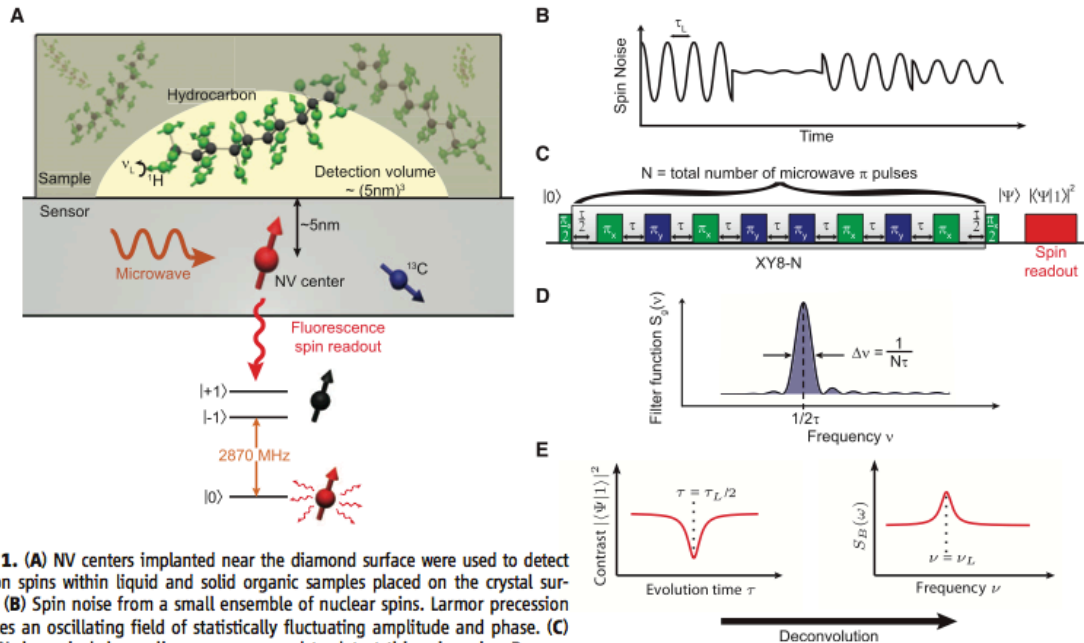


**Fig. 1.** (A) NV centers implanted near the diamond surface were used to detect proton spins within liquid and solid organic samples placed on the crystal surface. (B) Spin noise from a small ensemble of nuclear spins. Larmor precession creates an oscillating field of statistically fluctuating amplitude and phase. (C) XY8-N dynamical decoupling sequence used to detect this spin noise. Ramsey interferometry by an initial and final  $\pi/2$  pulse measures the magnetic field. A train of  $N$   $\pi$  pulses acts as a filter to select a specific frequency component of the noise. (D) Filter function of the pulse sequence, peaking at one specific frequency  $1/2\tau$ . (E) Repeating the sequence for varying pulse spacing  $\tau$  yields a spectrum of the spin noise.

Figure 7: Example of optical NMR, from [15].

## 6 Conclusions

All of the techniques presented image collections of cells in tissues, and in some of the techniques have spatial resolution sufficient to reveal the contents of cells. Though the techniques are diverse and rely on a number of different physical principles and mechanisms, they have a lot in common.

- Interference. Since the structures are small, the techniques need to find ways to extract information from waves that, at optical wavelengths, have wavelengths longer than the structures. In the case of nanoCT, though X rays are used, it is difficult to steer the X rays using traditional optics. In both cases, interference is used, whether in the fiber optic Michaelson interferometer of optical coherence tomography, or in the Fresnel lens that shape the beams used for nanocomputed tomography.
- Statistics. The super-resolution microscopies and NMR techniques do not defeat physical limits directly. Rather, by averaging over pixels in the case of super-resolution microscopy and spins in the case of NMR, aggregates can be averaged in a way to extract the information of interest. The square root of the number of measurements often appears as a consequence of the central limit theorem.
- “Interconversion” of time and space. In order to increase the spatial resolution of a technique, find out how to convert distance to path length, and then measure the time it takes light or some other medium to travel along the path; or if some process happens faster than can be measured, use a streak camera, or some other device that renders fast processes on multiple pixels to be recorded.

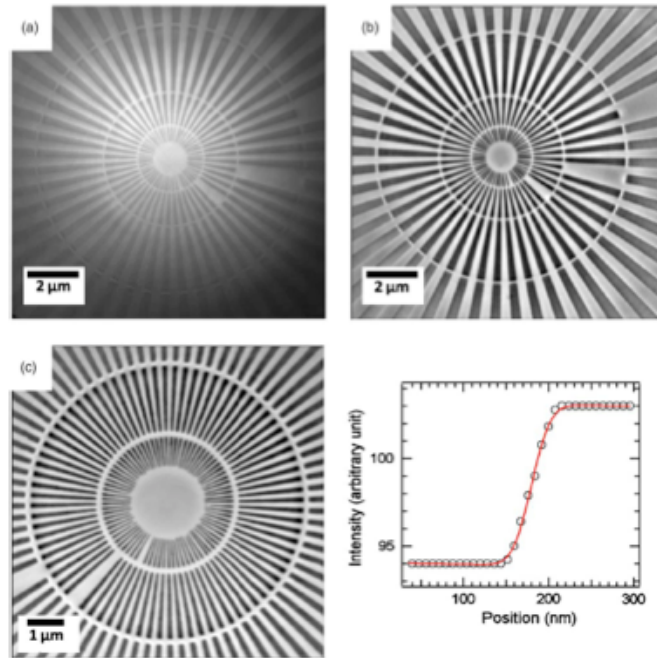


FIG. 1. (Color online) Images (a) and (b) are x-ray micrographs of a 650 nm thick Au Siemens star test pattern with an innermost feature width of 50 nm; (a) is an absorption image and (b) a Zernike phase contrast image. (c) Zernike phase contrast image of a 180 nm thick Au Siemens star test pattern with an innermost feature width of 30 nm. (d) An example of knife-edge intensity profile taken across a sharp feature of the test pattern. The Rayleigh resolution determined from the line profile is  $38.5 \pm 1.2$  nm.

Figure 8: Image of fabricated Fresnel lenses, from [16].

## References

- [1] Bo Huang, Mark Bates, and Xiaowei Zhuang. Super-Resolution Fluorescence Microscopy. *Annual Review of Biochemistry*, 78(1):993–1016, June 2009.
- [2] Silvio P Marchese Ragona and Philip G Haydon. Near-field Scanning Optical Microscopy and Near-field Confocal Optical Spectroscopy: Emerging Techniques in Biology. *Annals of the New York Academy of Sciences*, 820(1):196–207, 1997.
- [3] Aaron Lewis, Anna Radko, Nilly Ben Ami, Daniel Palanker, and Klony Lieberman. Near-field scanning optical microscopy in cell biology. *Trends in cell biology*, 9(2):70–73, 1999.
- [4] Yueli Chen, Laurel N Vuong, Jonathan Liu, Joseph Ho, Vivek J Srinivasan, Iwona Gorczynska, Andre J Witkin, Jay S Duker, Joel Schuman, and James G Fujimoto. Three-dimensional ultra-high resolution optical coherence tomography imaging of age-related macular degeneration. *Optics Express*, 17(5):4046, 2009.
- [5] G J Tearney. In Vivo Endoscopic Optical Biopsy with Optical Coherence Tomography. *Science*, 276(5321):2037–2039, June 1997.
- [6] Adolf F Fercher, Wolfgang Drexler, Christoph K Hitzenberger, and Theo Lasser. Optical coherence tomography-principles and applications. *Reports on progress in physics*, 66(2):239, 2003.

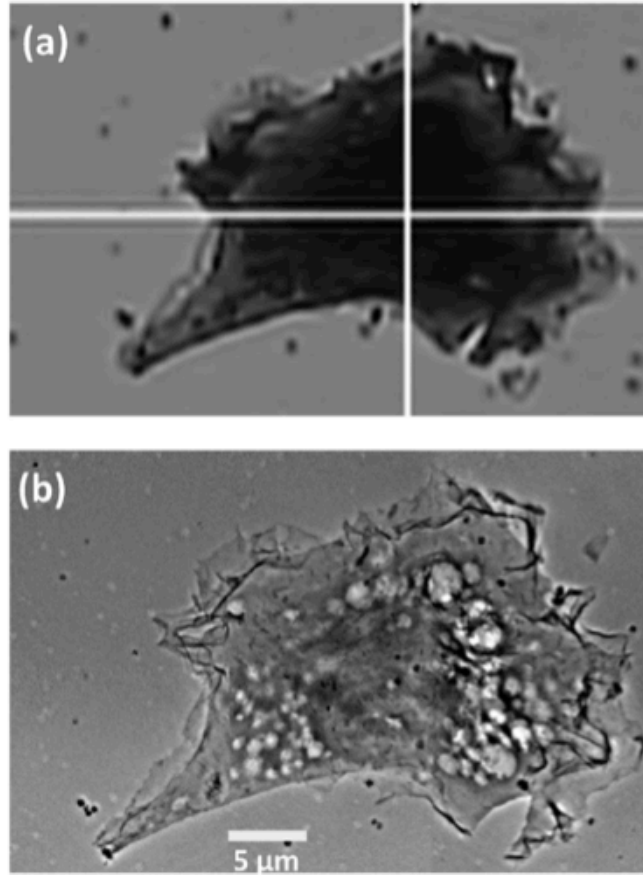


FIG. 3. (a) Optical image and (b) x-ray micrograph of the EMT cell, stained by B521-nickel, allowing the detection of subcellular structures.

Figure 9: NanoCT can reveal the internal structures of cells, from [16].

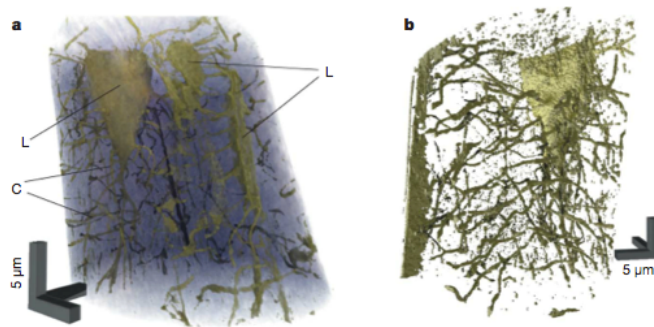


Figure 10: Reconstructed image of bone matrix based on nanoCT data, from [17].

[7] Evgenia Bousi, Ismini Charalambous, and Costas Pitris. Optical coherence tomography axial resolution improvement by step-frequency encoding. *Optics Express*, 18(11):11877–11890, 2010.

- [8] H Griffiths. Magnetic induction tomography. *Measurement science and technology*, 12(8):1126, 2001.
- [9] Eung Je Woo and Jin Keun Seo. Magnetic resonance electrical impedance tomography (MREIT) for high-resolution conductivity imaging. *Physiological Measurement*, 29(10):R1–R26, September 2008.
- [10] Hermann Scharfetter, Karl Hollaus, Javier Rosell-Ferrer, and Robert Merwa. Single-Step 3-D Image Reconstruction in Magnetic Induction Tomography: Theoretical Limits of Spatial Resolution and Contrast to Noise Ratio. *Annals of Biomedical Engineering*, 34(11):1786–1798, October 2006.
- [11] A Korjenevsky, V Cherepenin, and S Sapetsky. Magnetic induction tomography: experimental realization. *Physiological Measurement*, 21(1):89, 2000.
- [12] Yael G Maguire. Microslots: scalable electromagnetic instrumentation. 2004.
- [13] P Hemmer. Toward Molecular-Scale MRI. *Science*, 2013.
- [14] H J Mamin, M Kim, M H Sherwood, C T Rettner, and K Ohno. Nanoscale Nuclear Magnetic Resonance with a Nitrogen-Vacancy Spin Sensor. *Science*, 2013.
- [15] J Meijer, J Du, C A Meriles, F Reinhard, and J Wrachtrup. Nuclear Magnetic Resonance Spectroscopy on a (5-Nanometer) 3 Sample Volume. *Science*, 2013.
- [16] Y S Chu, J M Yi, F De Carlo, Q Shen, Wah-Keat Lee, H J Wu, C L Wang, J Y Wang, C J Liu, C H Wang, S R Wu, C C Chien, Y Hwu, A Tkachuk, W Yun, M Feser, K S Liang, C S Yang, J H Je, and G Margaritondo. Hard-x-ray microscopy with Fresnel zone plates reaches 40?nm Rayleigh resolution. *Applied Physics Letters*, 92(10):103119, 2008.
- [17] Martin Dierolf, Andreas Menzel, Pierre Thibault, Philipp Schneider, Cameron M Kewish, Roger Wepf, Oliver Bunk, and Franz Pfeiffer. Ptychographic X-ray computed tomography at the nanoscale. *Nature*, 467(7314):436–439, September 2010.
- [18] Alexander Sasov, Bart Pauwels, and Peter Bruyndonckx. New type of x-ray source for lensless laboratory nano-CT with 50-nm resolution. In Stuart R Stock, editor, *SPIE Optical Engineering + Applications*, pages 78040Q–78040Q–8. SPIE, August 2010.